Formation of highly uniform tin oxide nanochannels by electrochemical anodization on cold sprayed tin coatings

Mehdi Zarei [a], Salman Nourouzi [a,1], Roohollah Jamaati [a], Irene Garcia Cano [b], Sergi Dosta [b], Maria Sarret [b]

[a] Department of Materials Engineering, Babol Noshirvani University of Technology, Shariati Ave., 47148–71167 Babol, Iran

[b] Thermal Spray Centre, Department of Material Science and Physical Chemistry, Universitat de Barcelona, C/Martí i Franques 1, 08028 Barcelona, Spain

Abstract

In this study, the self-organized nanoporous tin oxide films were prepared on cold sprayed tin and tin foil through a voltage-controlled anodization method. The optimized cold spray parameters were used to obtain a dense structure. The morphology and crystallinity of the samples were investigated by FE-SEM and XRD, respectively. Firstly, an amorphous oxide film (SnO) with a compact and less regular outer layer and an almost regular and uniform inner layer was grown during anodization. This structure cause formation of close pores at the surface, which reduces the appropriate properties of the porous structure. Herein, a simple way to attain a totally open nanoporous structure is reported. Pulsed ultrasonic anodization ensured to be an effective way to create a mostly uniform open pores structure with few lateral inner cracks. It was found that the porous structure prepared on cold sprayed tin and tin foil are different because of the difference in

[1] Corresponding author
Email: s-nourouzi@nit.ac.ir

surface topography and imperfections. The current vs. time curves and the pores formation mechanism of cold sprayed tin and tin foil are discussed. The highest applicable annealing temperature for anodization of cold sprayed tin was 350°C. Nanoporous structure and adhesion to the substrate were maintained perfectly during the annealing at this temperature. Subsequent annealing at higher temperatures leads to the collapse of the pores structure.

Keywords: Tin oxide; Anodization; Cold spray; porous film; Oxalic acid

1. Introduction

Tin oxide (SnO_2) is a well-known n-type semiconductor with growing interest due to its electronic, optical, and photoelectrical properties that make it a promising material for wide potential applications in varistors[1,2], optoelectronics[3,4], catalysis[5], lithium-ion batteries[6], and sensors[7]. These applications desiderate a large specific surface area [8]. For this reason, anodization successfully adopted for the fabrication of nanostructured oxide layers on the surface of various metals such as Ti [9,10], Al [11,12], W [13], Zr [14], and Ta [15]. One of the advantages of the grown film by anodization is that most of the other methods need a supporting electrode to hold the materials to investigate electrochemically, but in anodization, the materials are used as the back contact electrode [16]. Anodization of Sn is a very interesting, simple, and cost-effective method to synthesize nanoporous tin oxide with large specific surface areas on the surface of metallic tin that was originally proposed by Shin et al. in 2004 [17]. Different parameters and solutions were used for anodizing a tin foil [18–22] and thin tin coatings [23–27].

Consistent with the previous reports [25,28], the resulting thin film from this process is amorphous tin oxide but, it is necessary to convert amorphous tin oxide to a crystalline form for use in most applications [29]. In most of the research, the post-annealing process has been used to transform amorphous nanochannels to polycrystalline SnO_2 [23,24,27,30]. But, the low melting point of Sn (∼230 °C) significantly hinders the formation of crystalline SnO_2 on the Sn support [17,31]. One way to bypass this hindrance is to deposit tin onto other substrates of higher melting points like copper [28] and SiO_2/Si [24]. This allows the tin to have stable support during the annealing process [28]. Nevertheless, annealing at high temperatures may transform nanoporous into particle-like structures [32] or delamination of the anodic oxide film from the tin substrate [28].

Cold spray is a deposition process in which solid-state particles accelerate to high velocities in a supersonic gas jet and deposit on the substrate [33]. The cold gas spray process uses high kinetic energy for the coating deposition. In this process, coatings are thick, with low porosity, without cracks (compressive stresses rather than tensile), and the oxidation is minimum [34].

To our knowledge, no nanoporous tin oxide films have been reportedly fabricated by anodization of cold sprayed tin. Concerning the possibility of using cold spray to prepare a dense coating on several substrates and for various applications, investigation of the anodization process on the coating prepared by this method would be interesting. Also, it is expected that anodized films on the cold sprayed tin have a different morphology and properties compared to foil and other kinds of coatings due to the different morphology and roughness of the surface. In this work, novel experimental findings were present of anodizing of cold sprayed tin. Several methods have been developed for preparing nanoporous tin on foil and coatings of tin. Finally, a new way is suggested to achieve the best microstructure of nanoporous tin by anodizing.

2. Experimental procedures

In this study, pure Sn powder was used as feedstock materials for cold spray. The scanning electron microscope (SEM) images of the feedstock powders are shown in Fig.1(a). The particle size distribution was measured using a laser scattering (Beckman Coulter LS 13 320) technique (Fig.1(b)). Before the deposition process, all substrates were grit blasted. The CGT KINETICS 4000 (Cold Gas Technology, Ampfing, Germany) equipment was used for the preparation of coating. The coatings were deposited on an aluminum substrate with the spraying parameters listed in Table1. The spray gun was mounted on a robot arm capable of moving three directions with respect to the surface of the substrate.

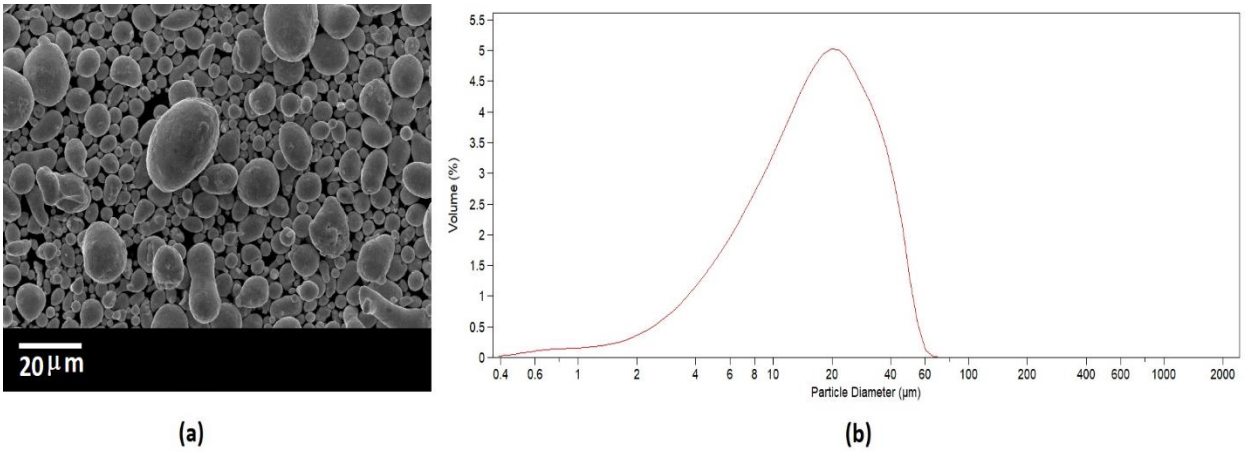

Fig. 1. (a) Morphology of the feedstock powders, (b) the particle size distribution was measured using a laser scattering.

Table 1. Spray parameters

Powder	Powder feed rate ($g.min^{-1}$)	Gas pressure (MPa)	Gas temperature (°C)	Stand-off (mm)	Traverse speed ($mm^{-1}s$)	Number of spray passes
Sn	25	7	200	40	250	2

The nanoporous tin oxide layers were electrochemically synthesized by anodization of cold sprayed tin coating and tin foil of 0.5 mm thick (Aldrich, 99.998%) at room temperature in a typical two-electrode system. Prior to anodizing, the samples were cleaned by ultrasonic baths containing a mixture of ethanol, acetone, and distilled water. Then, the samples were dried in the stream of warm air. The electrolyte of anodization was an oxalic acid (ALDRICH, 98%) aqueous solution without stirring or N_2 bubbling. To have the best control over the anodization process, 0.3 M was chosen for concentration, and the constant potential was applied for 600 s. The back of the samples

was sealed with insulating paint. A platinum wire was used as the cathode, and the distance between both electrodes was about 1 cm.

The applied potential has a significant effect on the surface morphologies of the samples [30]. Different amounts of potential were applied for anodic oxidation of cold sprayed tin using a Solartron 1285 potentiostat. After anodization, specimens were rinsed with deionized water. The anodic oxidation process was carried out with and without the ultrasonic, and current density vs. time curves were recorded during anodization.

The morphology and the compositions of anodized films were verified by using a JEOL JSM 5310 SEM and Field-Emission Scanning Electron Microscope (FE-SEM/EDS, JEOL JSM-7100F). Transmission electron microscope (TEM) image and selective area electron diffraction (SAED) pattern were taken with a JEM 2100 microscope, operated at 200 kV. For TEM characterization, a suspension prepared by dispersing a part of thin-film (scratched off from the surface of the tin substrate) was dropped on a holey carbon-supported copper grid. The crystallinity and phase composition films were analyzed by X-ray diffraction (XRD) measurements using an X'pert Philips MPD diffractometer (PANalytical) with monochromatic Cu Kα radiation (λ = 1.5418 Å) in a 10–120 2θ range. Finally, the anodic films were annealed to enhance the crystallinity.

3. Results and Discussion

The cross-sectional microstructure of the cold sprayed tin coatings is present in Fig. 2(a). It can be seen that continuous tin coatings were deposited, the coating is dense and uniform, and only small cracks might be observed near the substrate. The nonexistence of porosity and deformed splat structure demonstrate that appropriate parameters were used for the cold spray process to achieve a dense coating. The thickness of all examined tin coatings was around 120 μm.

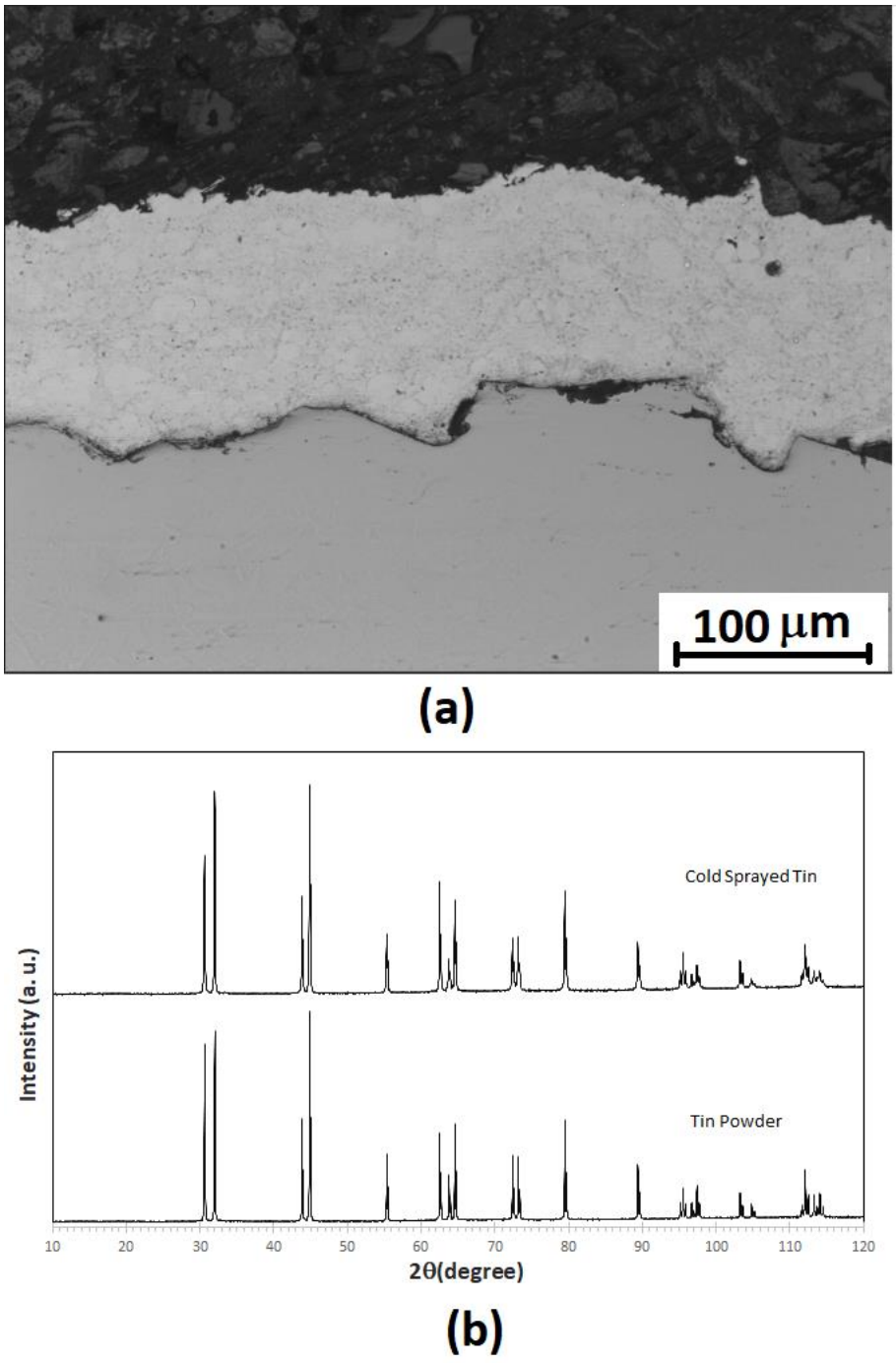

Fig. 2. (a) Optical micrograph showing the cross-section of the cold sprayed tin coating, (b) XRD spectra of tin powder and cold sprayed tin coating

X-ray diffraction patterns of tin powder and cold sprayed tin coating are collected in Fig. 2(b). The same pure tin pattern with no spectacular changes in both of the samples indicates that no preferred orientation has occurred during the cold spray process.

In the case of cold sprayed tin, similar to tin foil [19], the anodization by potential between 4 and 8 V resulted in the formation of nanoporous tin oxide film independently of the electrolyte concentration. The top surface of as-anodized tin coatings at the potentials of 4V, 6V, and 8V are shown in Fig. 3.

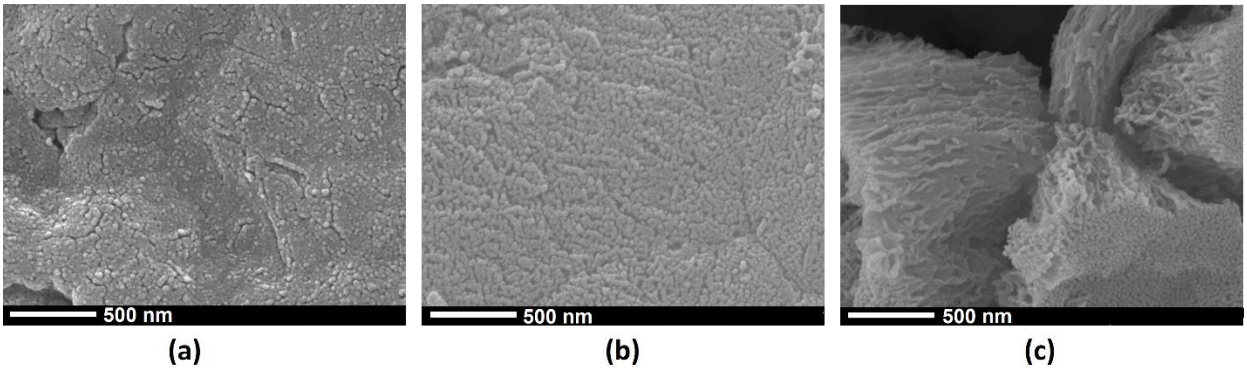

Fig. 3. FESEM images of tin oxide films synthesized in 0.3 M oxalic acid electrolyte for 600 s at the potentials of (a) 4, (b) 6, and (c) 8 V.

At the lowest potential, the surface is rough and inhomogeneity of the surface has been made by anisotropic and slow anodization (Fig. 3(a)). In some parts, micron-sized particles were formed similar to what was observed in the other study [19]. Wang et al. identified SnC_2O_4 in this condition [18]. As seen in Fig. 3(b), higher potential (6 V) enhances the number of initiation sites and rapid growth. However, further increasing the potential led to dissolving the oxide walls in acid solution. As well as by exorbitance potential (8 V), the adhesion of the film to the substrate decrease because of more vigorous O_2 evolution at the interface of film/substrate and result in delamination of film from the substrate during the anodizing or subsequence drying [17]. Also, the

number of internal cracks increases significantly with increasing the potential of anodization, similar to those observed by Lee et al. [26]. In this potential, the layer is destroyed by vigorous oxygen evolution under severe anodizing conditions (Fig. 3(c)). Taking the above consideration, it seems that the appropriate potential for the formation of uniform porous is 6 V.

The current density versus time (i-t) plot was recorded during anodization of tin at different potentials are shown in Fig. 4(a). As can be seen, two types of curves appear in the figures:

Type I: A rapid decrease in the first stage of anodization to a minimum is observed. Afterward, a constant level of current density can be observed until the end of the anodization process.

Type II: At the start of the anodization process, the current density decreases rapidly to a minimum level of current density. Afterward, a gradual increase in current density to a maximum is observed, and then the current density attains a steady-state current density.

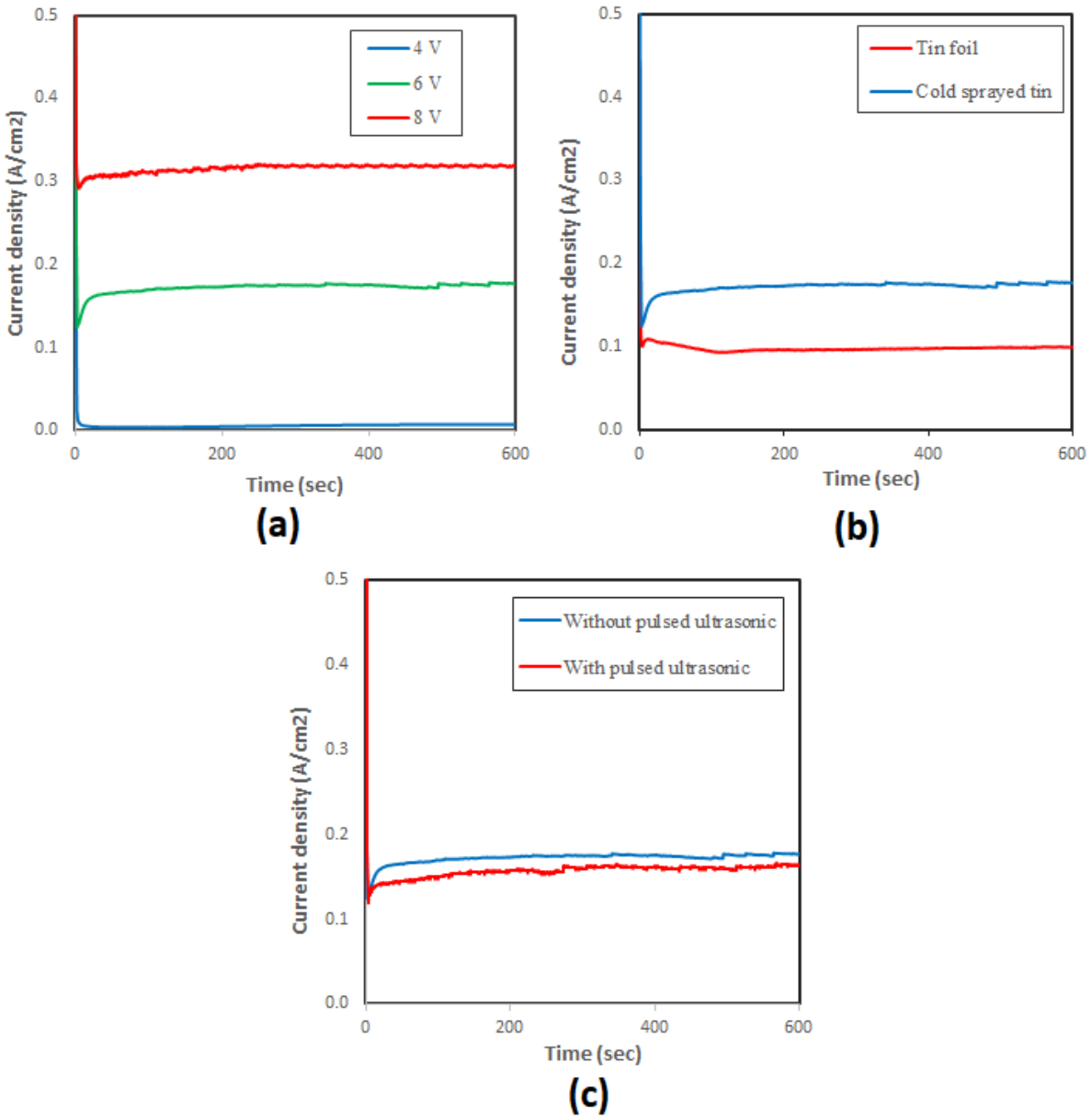

Fig. 4. (a) Current transient during anodization of (a) cold sprayed tin coating at three different potentials, (b) cold sprayed tin coating and tin foil,(c) cold sprayed tin coating with pulsed ultrasonic and without ultrasonic

Such behavior can be ascribed to different stages of the pore formation procedure. Generally, this process can be divided into some stages:

At the first stage, a passive layer is formed on the metal surface, leading to a quick decrease of current density to a minimum level. After this stage, the passive layer is breakdown locally and the active area increases due to the pores start to form and grow. This process is accompanied by a gradual increase in current density. After this stage, with the extension of the anodization, the individual pores start to compete for the available current. Under optimized conditions, a situation arises where the pores equally share the available current, the current density decreases gently and a steady-state current density of generation of nanoporous oxide occurs [35–37]. Similar behavior was reported by Zaraska et al. [21] during anodization of tin foil in NaOH solution at low applied voltages. At the potential of 4 V, the minimum and maximum of the curve are not so evident. After the formation of the passive layer, no breakdown of the passive layer occurred even after the 600 s. The profile of current transient during the anodization of Sn at 6 V is similar to that of other well-known metals [37,38], with this difference that because of the faster reaction process, the time-scale in anodization of tin is significantly shorter than others [39]. As expected, by increasing the potential, much higher current densities appeared. At this condition, after forming and growing pores, the high potential leads to higher corrosion and does not allow the growth of channels to increase. Therefore, there is a slight difference between the lowest current density and the steady-state current density.

Fig. 4(b) shows the current density-time curves of anodization of cold sprayed tin coating and tin foil at the same anodization condition. As can be seen, a significant drop in current density is observed in both samples due to the initial formation of the compact layer. However, the local minimum of current density in the case of tin foil is lower than the deposited tin. It can be attributed to the fact that more imperfections in cold sprayed samples surface led to more pores precursors through the barrier film. Therefore, by increasing these individual paths, the current density begins

to rise sooner. On the other hand, the deep of current density vs. time curve (the difference between minimum current density and steady-state current density) in the case of cold sprayed is much more than the foil case because more pores in the surface of cold sprayed tin led to more enhancement in current density.

At anodization with an applied potential of 6 V on the cold sprayed tin, small pores appear with almost regular morphology, but it seems the surface of pores is closed. Regarding other studies, anodization of tin oxide in oxalic acid electrolytes, even under typical anodizing conditions, can lead to forming completely closed surface pores, especially at anodic oxidation of Sn deposited on other conductive substrates [32]. Nanosized pores could be seen under the compact layer (Fig. 5(a)), demonstrating that nanosized pores were closed at the end stage of the anodization. This situation has been observed in the porous SnO_2 films were prepared by anodization of tin thin films deposited on SiO_2/Si substrates [24] and in anodizing of high current tin deposit [26].

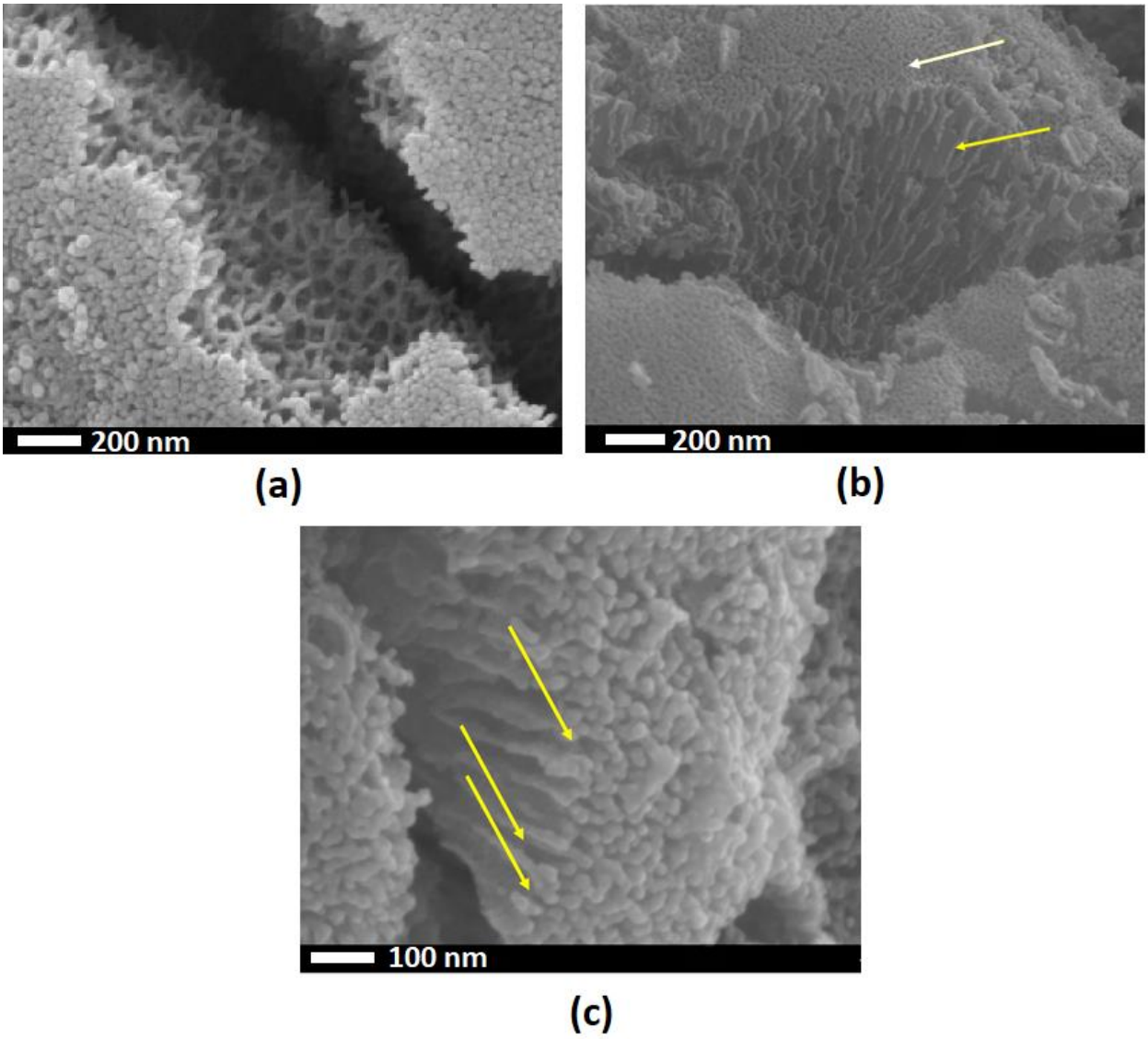

Fig. 5. FESEM image of (a) the compact and nanoporous tin oxide film synthesized at the potential of 6 V, in 0.3 M oxalic acid electrolyte for 600 s, (b) a cross-sectional view of anodic tin oxide film formed at the same conditions. Inner porous: yellow arrow and outer porous: white arrow, (c) corrosion behavior of tin oxide walls

FESEM image of a cross-sectional view of anodic tin oxide film formed by anodization of cold sprayed tin coating during 600 s in 0.3 M oxalic acid electrolyte and at the potential of 6V is shown in Fig. 5(b). As can be seen, the diameter of the outer pores of the tin oxide film is much smaller

than the diameter of the inner pores. In consequence, the porous structure was almost completely blocked to the outside. In this structure, the appropriate properties of the porous structure cannot be expected because access to internal pores is only available via structural imperfections [26]. This occurrence is because of the accumulation of oxygen in the generated pores, which does not escape quickly from the oxide film during the anodization process. This accumulated oxygen acts as a mold and leads to enhance internal pore size [40]. Besides, with careful observation of the cross-section of outer pores, a mechanism for the shape of the outer layer can be proposed. As shown in Fig. 5(c), it seems during the growing of pores, some parts of the walls were corroded faster. The closer look indicates that the junctions of the separate pores are partly more resistant to corrosion. It should be additionally mentioned that more vigorous gas evolution during electrolysis can increase the irregularity of corrosion of walls.

The intermittent potential was suggested to avoid producing these close surface channels during the anodization of tin [26]. The same procedure was applied to the cold sprayed tin coating. Some nanochannels appeared in some parts of the surface, but the surface of the tin substrate was not uniformly anodized over large areas. Also, achieving a highly uniform SnO_2 nanochannels was suggested by using ultrasonic anodization on tin foil [39]. This process makes some suitable results in the formation of an open porous structure of cold sprayed tin coatings, but it seems that modifying this process can lead to the formation of a nanochannel structure with long-range order. Applying ultrasonic waves succor the oxygen gas escaping smoothly, leading to the formation of a homogeneous distribution of chemical SnO_2 layers throughout the whole surface and preventing the generation of lateral cracks [39].

A modification process was used in this study to prepare an appropriate open nanoporous structure on the whole surface of anodized cold sprayed tin. The FESEM images of the nanoporous tin film

prepared by pulsed ultrasonic anodization process on cold sprayed tin and tin foil are shown in Fig. 6. It was observed that using pulsed ultrasonic during the anodization method leads to the preparation of a surface with a high amount of the quite uniform open nanoporous (Figs. 6(a) and 6(b)). Along with the benefits of the ultrasonic, using the pulsed method to apply these waves sever the accumulated oxygen gas in the channels and help them for escaping faster and easier. The microstructure images of the as-anodized film prepared by this method on tin foil are shown in Fig. 6(c) and 6(d). It is seen that vertically aligned nanochannels SnO2 was achieved, and the anodic oxidation film is highly uniform and porous, but the porous diameter in the case of tin foil is larger than the case of cold sprayed tin. The reason for these differences can be explained by the number of embryo pores through the barrier film in the cold sprayed tin. More embryo pores lead to having more pores per unit area with fewer diameters.

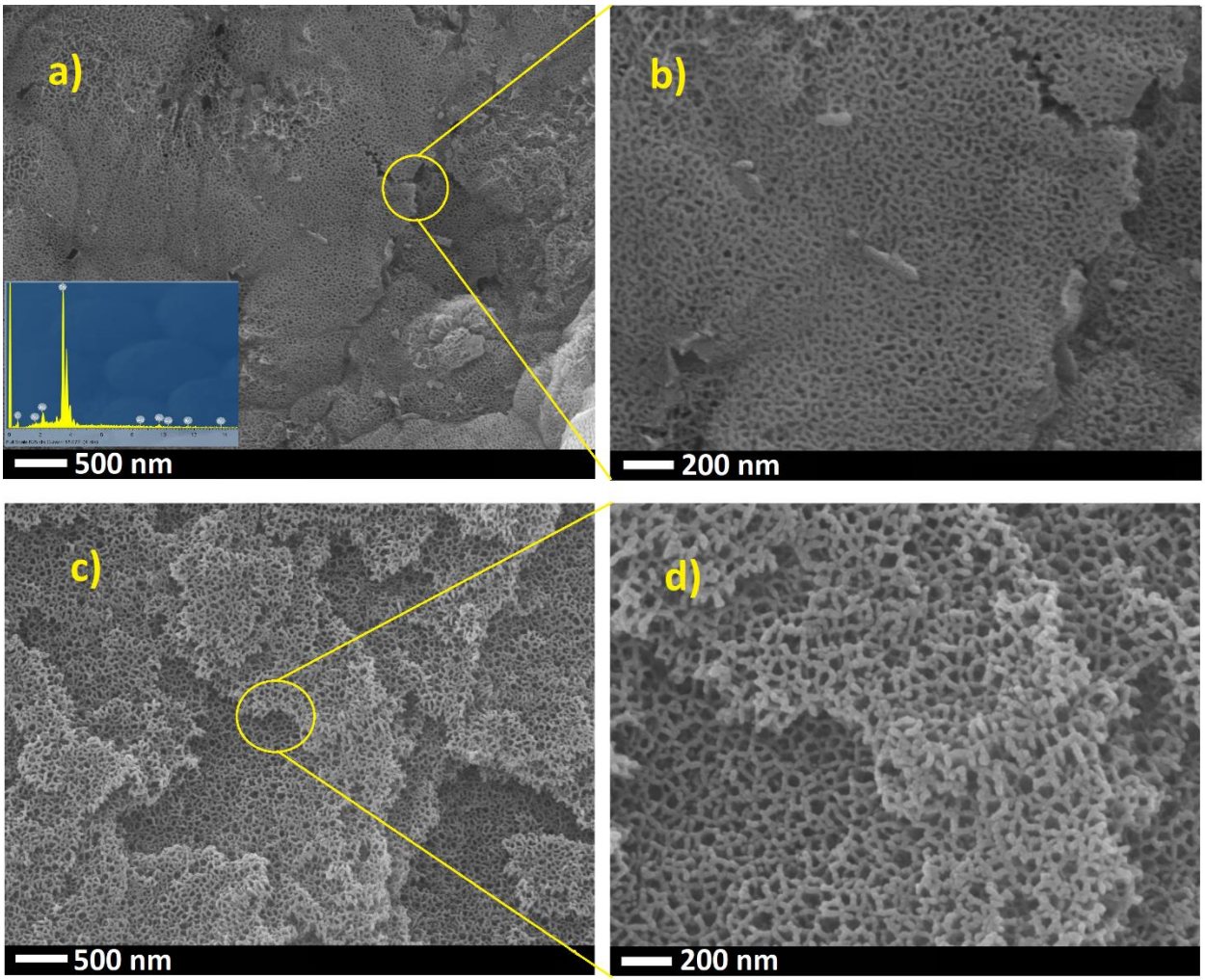

Fig. 6. FESEM images of the nanoporous tin film prepared by pulsed ultrasonic anodization process on (a,b) cold sprayed tin, and (c,d) tin foil.

The typical current density - time (i − t) curves of the anodization samples with pulsed ultrasonic and without pulse ultrasonic anodization are shown in Fig. 4(c). A rapid decrease in the recorded current density to the same level occurred in both samples. However, the breakdown of the passive layer and the formation of the porous oxide structure were distinct. After the formation of nanochannels, applied pulsed ultrasonic wave leads to prevent forming a dense outer layer, which

is responsible for higher current density in a simple way. Consequently, the current density reaches a steady-state without a significant increase.

As shown in Fig. 7, the as-anodized cold sprayed tin film was characterized by transmission electron microscopy–selected area electron diffraction (TEM-SAED). The weak continuous ring in the pattern of this sample implies low-ordered, amorphous, or poorly crystalline materials [28]. The X-ray diffraction (XRD) patterns of the tin oxide film are collected in Fig. 8(a). Belonging all peaks in the XRD pattern of the as-anodized film to the metallic tin substrate and the broad feature of XRD spectra (comparing to the XRD result of coating sample at Fig. 2(b)) imply to amorphous nature of tin oxide film. Therefore, according to the results of XRD, the result of TEM-SAED, the dark color of the oxide layer, and the atomic ratio of Sn and O (1:1) obtained from EDS (Fig. 6), it can be concluded that amorphous SnO was formed as a result of anodization.

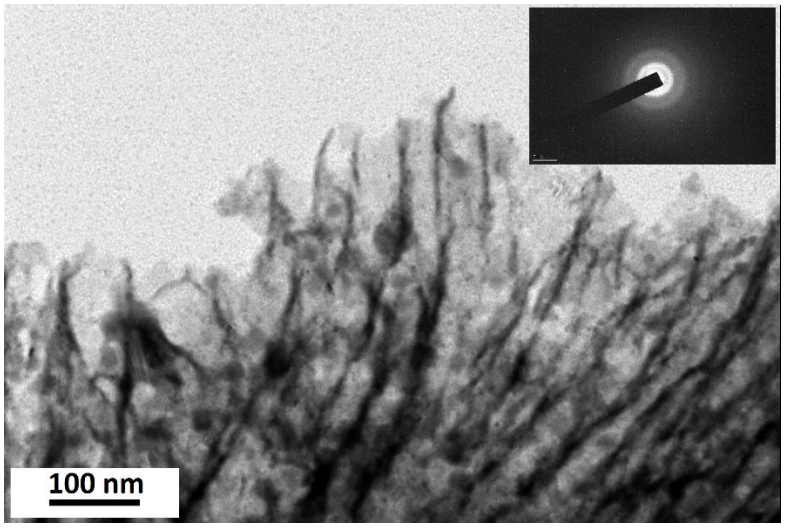

Fig. 7. TEM image and SAED pattern of as-anodized cold sprayed tin nanochannel structure.

Annealing of the amorph tin oxide film is limited because the tin sub-layer has a low melting point (~230 °C). It has been reported that it is possible to anneal this film up to 400 °C and preserve the

channel structure for all temperatures because between melting temperature and 400 °C, a liquid pool of tin is formed that confined by the outer oxide layer and protects it from further melting [28,32]. It was reported that after 400 °C, the anodic oxide layer peeled off from the substrate [28]. However, Jeun et al. [24] reported annealing at higher temperatures (up to 700 °C) by complete anodization of tin, which is evaporated on SiO_2/Si substrates. In this study, the appropriate nanoporous structure of tin oxide on the Sn substrate was obtained during annealing up to 350 °C. Almost no change in the oxide morphology during annealing at this temperature was observed. Annealing at the higher temperatures led to the collapse of the pore structure of anodic oxide film, and at the higher than 400 °C lead to peeling off the porous film from the tin substrate.

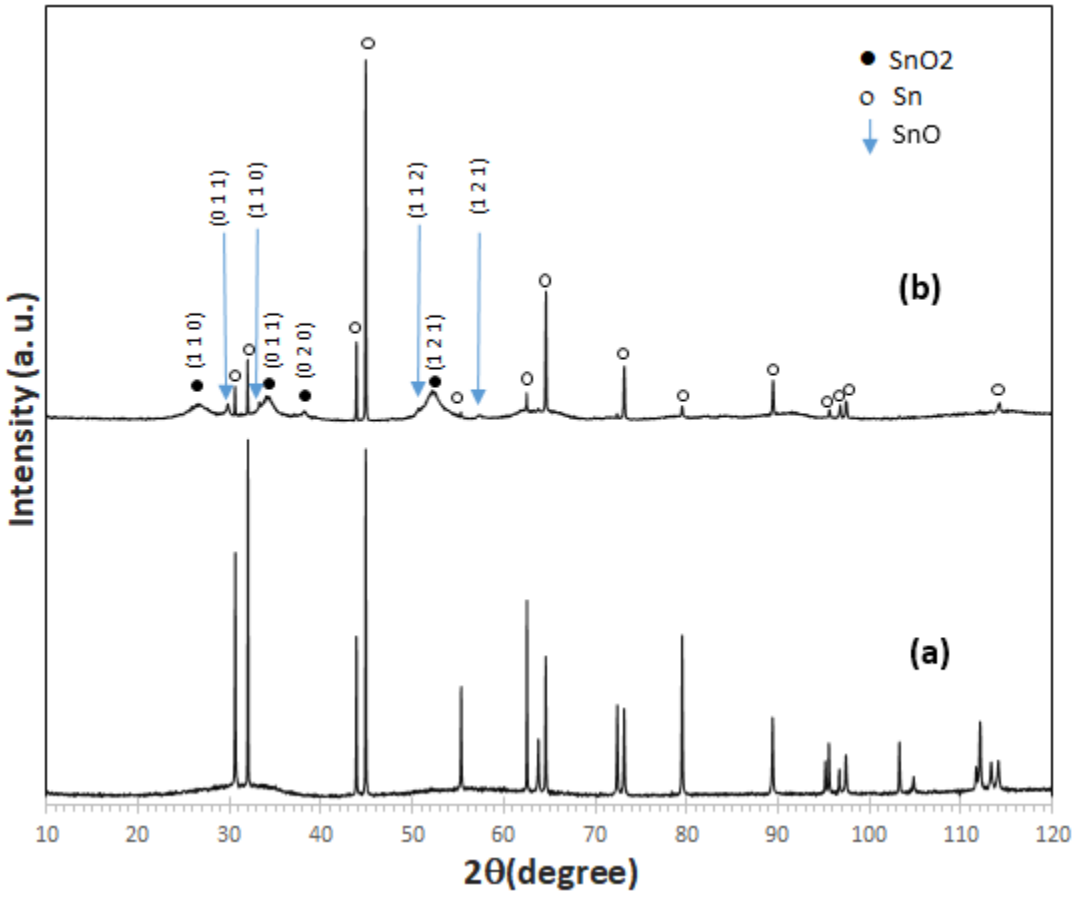

Fig. 8. XRD pattern of (a) as-anodized cold sprayed tin and (b) annealed sample at 350 °C.

Besides the characteristic peaks of the tin substrate, the XRD pattern of annealed tin oxide film at temperatures 350 °C (Fig. 8(b)) exhibits four broad peaks at about 26.5°, 34°, 38°, and 52°, which correspond quite well to tetragonal SnO_2. These peaks are in respect to (1 1 0), (0 1 1), (0 2 0), and (1 2 1) planes, respectively. In addition, four small peaks (blue arrows) appear in the region of 2θ around 30°, 33.5°, 50.5°, and 57.5° reveal the presence of crystalline SnO. These peaks can be indexed to the (0 1 1), (1 1 0), (1 1 2), and (1 2 1) planes, respectively. The building units of tin oxide amorphous are SnO_6 octahedra with Sn cation surrounded by six oxygen anions. These octahedra units are randomly distributed in the amorphous structures and can be rearranged into ordered lattice structures by heat treatment[29]. In addition to rutile SnO_2, the annealing procedure in this study led to the formation of crystalline tetragonal SnO. This phase was observed during annealing of the tin oxide film in some studies [23,28,30], but, with regard to the results of the annealing at higher temperature [23,24,28,30,32], this phase disappears at the temperature above 400 °C.

4. Conclusions

In summary, nanoporous tin oxide films have been prepared on cold sprayed tin coatings and tin foil using an anodic oxidation process. The closed surface pores observed in typical anodic porous tin oxides were obtained in these layers. A modified procedure to prepare nanoporous tin oxide films with vertical open pores have been presented. It was demonstrated that using a pulsed ultrasonic wave during anodization is an accomplishable way to form a surface with open and long-range order nanochannels. The results confirmed that the structure of the pores prepared by the same procedure in cold sprayed tin and tin foil is different because of the presence of much more imperfection on the surface of the cold sprayed coating samples. The maximum applicable

temperature for annealing of the cold sprayed tin was 350 °C. Up to this temperature, the open porous structure of these films remained perfectly. The nature of the as-anodized film was amorphous SnO, and the annealing process led to the formation of crystalline rutile SnO_2 and tetragonal SnO. Such nanoporous oxides could be excellent candidates for various applications. This study might be a first step towards preparing tin oxide film on cold sprayed tin coatings, which may discover application in functional devices. Also, it will be interesting to prepare Sn coatings with different thicknesses to investigate the contribution of the substrate and the interface on the morphology of the film.

Data availability

All data included in this study are available upon request by contact with the corresponding author.

References

[1] Liang, W., Zhao, H., Meng, X., Fan, S., and Xie, Q., 2021, "High Nonlinearity and Low Leakage Current SnO2 Varistor Ceramics by Co-Doping with Yttrium and Tantalum," Mater. Lett., **285**, p. 129120.

[2] Zhao, H., Liang, W., Wang, F., Zhou, Y., and Xie, Q., 2020, "A Low Leakage Current (Co, Mn, Ta)-SnO2 Varistor Tailored by Doping with Chromium for Power Grids," Results Phys., **18**, p. 103314.

[3] Powell, M. J., Williamson, B. A. D., Baek, S.-Y., Manzi, J., Potter, D. B., Scanlon, D. O., and Carmalt, C. J., 2018, "Phosphorus Doped SnO2 Thin Films for Transparent

Conducting Oxide Applications: Synthesis, Optoelectronic Properties and Computational Models," Chem. Sci., **9**(41), pp. 7968–7980.

[4] Kumar, P., Khadtare, S., Park, J., and Yadav, B. C., 2020, "Fabrication of Leaf Shaped SnO2 Nanoparticles via Sol–Gel Route and Its Application for the Optoelectronic Humidity Sensor," Mater. Lett., **278**, p. 128451.

[5] Manjunathan, P., Marakatti, V. S., Chandra, P., Kulal, A. B., Umbarkar, S. B., Ravishankar, R., and Shanbhag, G. V, 2018, "Mesoporous Tin Oxide: An Efficient Catalyst with Versatile Applications in Acid and Oxidation Catalysis," Catal. Today, **309**, pp. 61–76.

[6] Versaci, D., Costanzo, A., Ronchetti, S. M., Onida, B., Amici, J., Francia, C., and Bodoardo, S., 2021, "Ultrasmall SnO2 Directly Grown on Commercial C45 Carbon as Lithium-Ion Battery Anodes for Long Cycling Performance," Electrochim. Acta, **367**, p. 137489.

[7] Das, S., Girija, K. G., Debnath, A. K., and Vatsa, R. K., 2021, "Enhanced NO2 and SO2 Sensor Response under Ambient Conditions by Polyol Synthesized Ni Doped SnO2 Nanoparticles," J. Alloys Compd., **854**, p. 157276.

[8] Batzill, M., and Diebold, U., 2005, "The Surface and Materials Science of Tin Oxide," Prog. Surf. Sci., **79**(2), pp. 47–154.

[9] Macák, J. M., Tsuchiya, H., and Schmuki, P., 2005, "High-Aspect-Ratio TiO2 Nanotubes by Anodization of Titanium," Angew. Chemie Int. Ed., **44**(14), pp. 2100–2102.

[10] Shankar, K., Mor, G. K., Prakasam, H. E., Yoriya, S., Paulose, M., Varghese, O. K., and Grimes, C. A., 2007, "Highly-Ordered TiO2nanotube Arrays up to 220 Mm in Length: Use in Water Photoelectrolysis and Dye-Sensitized Solar Cells," Nanotechnology, **18**(6),

p. 65707.

[11] Sulka, G. D., and Parkoła, K. G., 2007, “Temperature Influence on Well-Ordered Nanopore Structures Grown by Anodization of Aluminium in Sulphuric Acid,” Electrochim. Acta, **52**(5), pp. 1880–1888.

[12] Sulka, G. D., and Parkoła, K. G., 2006, “Anodising Potential Influence on Well-Ordered Nanostructures Formed by Anodisation of Aluminium in Sulphuric Acid,” Thin Solid Films, **515**(1), pp. 338–345.

[13] Zheng, H., Sadek, A. Z., Latham, K., and Kalantar-Zadeh, K., 2009, “Nanoporous WO3 from Anodized RF Sputtered Tungsten Thin Films,” Electrochem. commun., **11**(4), pp. 768–771.

[14] Tsuchiya, H., and Schmuki, P., 2004, “Thick Self-Organized Porous Zirconium Oxide Formed in H2SO4/NH4F Electrolytes,” Electrochem. commun., **6**(11), pp. 1131–1134.

[15] El-Sayed, H. A., and Birss, V. I., 2009, “Controlled Interconversion of Nanoarray of Ta Dimples and High Aspect Ratio Ta Oxide Nanotubes,” Nano Lett., **9**(4), pp. 1350–1355.

[16] Shinde, D. V, Lee, D. Y., Patil, S. A., Lim, I., Bhande, S. S., Lee, W., Sung, M. M., Mane, R. S., Shrestha, N. K., and Han, S.-H., 2013, “Anodically Fabricated Self-Organized Nanoporous Tin Oxide Film as a Supercapacitor Electrode Material,” RSC Adv., **3**(24), pp. 9431–9435.

[17] Shin, H.-C., Dong, J., and Liu, M., 2004, “Porous Tin Oxides Prepared Using an Anodic Oxidation Process,” Adv. Mater., **16**(3), pp. 237–240.

[18] Wang, M., Liu, Y., Zhang, D., and Yang, H., 2012, “Anodization Process of Sn in Oxalic Acid at Low Applied Voltages,” Electrochim. Acta, **59**, pp. 441–448.

[19] Zaraska, L., Bobruk, M., Jaskuła, M., and Sulka, G. D., 2015, “Growth and Complex

Characterization of Nanoporous Oxide Layers on Metallic Tin during One-Step Anodic Oxidation in Oxalic Acid at Room Temperature," Appl. Surf. Sci., **351**, pp. 1034–1042.

[20] Lu, C., Wang, J., Meng, D., Wang, A., Wang, Y., and Zhu, Z., 2016, "Tunable Synthesis of Nanoporous Tin Oxide Structures on Metallic Tin by One-Step Electrochemical Anodization," J. Alloys Compd., **685**, pp. 670–679.

[21] Zaraska, L., Gilek, D., Gawlak, K., Jaskuła, M., and Sulka, G. D., 2016, "Formation of Crack-Free Nanoporous Tin Oxide Layers via Simple One-Step Anodic Oxidation in NaOH at Low Applied Voltages," Appl. Surf. Sci., **390**, pp. 31–37.

[22] Wang, M., Liu, Y., Xue, D., Zhang, D., and Yang, H., 2011, "Preparation of Nanoporous Tin Oxide by Electrochemical Anodization in Alkaline Electrolytes," Electrochim. Acta, **56**(24), pp. 8797–8801.

[23] Zaraska, L., Gawlak, K., Wiercigroch, E., Malek, K., Kozieł, M., Andrzejczuk, M., Marzec, M. M., Jarosz, M., Brzózka, A., and Sulka, G. D., 2019, "The Effect of Anodizing Potential and Annealing Conditions on the Morphology, Composition and Photoelectrochemical Activity of Porous Anodic Tin Oxide Films," Electrochim. Acta, **319**, pp. 18–30.

[24] Jeong-Hoon Jeun, Hyun-Sam Ryu, and S.-H. H., 2009, "Nanoporous SnO2 Film Gas Sensor Formed by Anodic Oxidation," J. Electrochem. Soc., **156**(9), pp. J263–J266.

[25] Zaraska, L., Czopik, N., Bobruk, M., Sulka, G. D., Mech, J., and Jaskuła, M., 2013, "Synthesis of Nanoporous Tin Oxide Layers by Electrochemical Anodization," Electrochim. Acta, **104**, pp. 549–557.

[26] Lee, J.-W., Park, S.-J., Choi, W.-S., and Shin, H.-C., 2011, "Well-Defined Meso- to Macro-Porous Film of Tin Oxides Formed by an Anodization Process," Electrochim.

Acta, **56**(17), pp. 5919–5925.

[27] Li, J., Wang, J., Zhang, L., and Zhang, S., 2015, "Nanocrystalline SnO 2 Thin Films Prepared by Anodization of Sputtered Sn Thin Films," J. Vac. Sci. Technol. A Vacuum, Surfaces, Film., **33**(3), p. 031508.

[28] Palacios-Padrós, A., Altomare, M., Lee, K., Díez-Pérez, I., Sanz, F., and Schmuki, P., 2014, "Controlled Thermal Annealing Tunes the Photoelectrochemical Properties of Nanochanneled Tin-Oxide Structures," ChemElectroChem, **1**(7), pp. 1133–1137.

[29] Bian, H., Dong, R., Shao, Q., Wang, S., Yuen, M.-F., Zhang, Z., Yu, D. Y. W., Zhang, W., Lu, J., and Li, Y. Y., 2017, "Water-Enabled Crystallization of Mesoporous SnO2 as a Binder-Free Electrode for Enhanced Sodium Storage," J. Mater. Chem. A, **5**(45), pp. 23967–23975.

[30] Chen, H., Zhu, W., Zhou, X., Zhu, J., Fan, L., and Chen, X., 2011, "Formation of Porous SnO2 by Anodic Oxidation and Their Optical Properties," Chem. Phys. Lett., **515**(4–6), pp. 269–273.

[31] Zaraska, L., Bobruk, M., and Sulka, G. D., 2015, "Formation of Nanoporous Tin Oxide Layers on Different Substrates during Anodic Oxidation in Oxalic Acid Electrolyte," Adv. Condens. Matter Phys., **2015**, p. 302560.

[32] Zaraska, L., Syrek, K., Hnida, K. E., Bobruk, M., Krzysik, A., Łojewski, T., Jaskuła, M., and Sulka, G. D., 2016, "Nanoporous Tin Oxides Synthesized via Electrochemical Anodization in Oxalic Acid and Their Photoelectrochemical Activity," Electrochim. Acta, **205**, pp. 273–280.

[33] Zahiri, S. H., Fraser, D., and Jahedi, M., 2009, "Recrystallization of Cold Spray-Fabricated CP Titanium Structures," J. Therm. Spray Technol., **18**(1), pp. 16–22.

[34] SILVA, F. S. da et al., 2018, “Cold Gas Spray Coatings: Basic Principles Corrosion Protection and Applications.,” Eclética Química J., **42**(1), pp. 09–32.

[35] Sulka, G. D., 2008, “Highly Ordered Anodic Porous Alumina Formation by Self-Organized Anodizing,” Nanostructured Mater. Electrochem., pp. 1–116.

[36] Macak, J. M., Tsuchiya, H., Ghicov, A., Yasuda, K., Hahn, R., Bauer, S., and Schmuki, P., 2007, “TiO2 Nanotubes: Self-Organized Electrochemical Formation, Properties and Applications,” Curr. Opin. Solid State Mater. Sci., **11**(1), pp. 3–18.

[37] Sulka, G. D., Kapusta-Kołodziej, J., Brzózka, A., and Jaskuła, M., 2010, “Fabrication of Nanoporous TiO2 by Electrochemical Anodization,” Electrochim. Acta, **55**(14), pp. 4359–4367.

[38] Lee, W., and Park, S.-J., 2014, “Porous Anodic Aluminum Oxide: Anodization and Templated Synthesis of Functional Nanostructures,” Chem. Rev., **114**(15), pp. 7487–7556.

[39] Kim, J.-Y., Kang, J. S., Shin, J., Kim, J., Han, S.-J., Park, J., Min, Y.-S., Ko, M. J., and Sung, Y.-E., 2015, “Highly Uniform and Vertically Aligned SnO2 Nanochannel Arrays for Photovoltaic Applications,” Nanoscale, **7**(18), pp. 8368–8377.

[40] Cao, J., Gao, Z., Wang, C., Muzammal, H. M., Wang, W., Gu, Q., Dong, C., Ma, H., and Wang, Y., 2020, “Morphology Evolution of the Anodized Tin Oxide Film during Early Formation Stages at Relatively High Constant Potential,” Surf. Coatings Technol., **388**, p. 125592.